The Journal of Immunology

TLR3–Responsive, XCR1$^+$, CD141(BDCA-3)$^+$/CD8α^+-Equivalent Dendritic Cells Uncovered in Healthy and Simian Immunodeficiency Virus–Infected Rhesus Macaques

Charles-Antoine Dutertre, Jean-Pierre Jourdain, Magali Rancez, Sonia Amraoui, Even Fossum, Bjarne Bogen, Cindy Sanchez, Anne Couëdel-Courteille, Yolande Richard, Marc Dalod, Vincent Feuillet, Rémi Cheynier and Anne Hosmalin

J Immunol 2014; 192:4697-4708; Prepublished online 16 April 2014;
doi: 10.4049/jimmunol.1302448
http://www.jimmunol.org/content/192/10/4697

The Journal of Immunology is published twice each month by
The American Association of Immunologists, Inc.,
1451 Rockville Pike, Suite 650, Rockville, MD 20852

Print ISSN: 0022-1767 Online ISSN: 1550-6606.

TLR3–Responsive, XCR1$^+$, CD141(BDCA-3)$^+$/CD8α$^+$-Equivalent Dendritic Cells Uncovered in Healthy and Simian Immunodeficiency Virus–Infected Rhesus Macaques

Charles-Antoine Dutertre,[*,†,‡,1] Jean-Pierre Jourdain,[*,†,‡,2] Magali Rancez,[*,†,‡,2] Sonia Amraoui,[*,†,‡] Even Fossum,[§] Bjarne Bogen,[§,¶] Cindy Sanchez,[‖,#,] Anne Couëdel-Courteille,[*,†,‡] Yolande Richard,[*,†,‡] Marc Dalod,[‖,#,**] Vincent Feuillet,[*,†,‡] Rémi Cheynier,[*,†,‡,3] and Anne Hosmalin[*,†,‡,††,3]**

In mice, CD8α$^+$ myeloid dendritic cells (mDC) optimally cross-present Ags to CD8$^+$ T cells and respond strongly to TLR3 ligands. Although equivalent DC have been identified by comparative genomic analysis and functional studies in humans as XCR1$^+$CD141 (BDCA-3)$^+$Clec9A$^+$cell adhesion molecule 1$^+$ mDC, and in sheep as CD26$^+$ mDC, these cells remained elusive in nonhuman primates. To remedy this situation, we delineated precisely DC and monocyte populations by 12-color flow cytometry and transcriptomic analyses in healthy rhesus macaques. We identified a new mDC population, with strong phenotypic and transcriptional homology to human CD141$^+$ and murine CD8α$^+$ mDC, including XCR1 membrane expression as a conserved specific marker. In contrast, high CD11c expression was not characteristic of mDC in macaques, but of CD16$^+$ monocytes. Like their human and murine homologs, simian XCR1$^+$ mDC had much stronger responses to TLR3 stimulation than other myeloid cells. The importance of this new mDC population was tested in SIV$_{mac251}$ infection, the most relevant animal model for pathogenic HIV-1 infection and vaccination. This population increased sharply and transiently during acute infection, but was reduced in blood and spleen during advanced disease. The identification of XCR1$^+$ mDC in rhesus macaques opens new avenues for future preclinical vaccinal studies and highlights XCR1 as a prime candidate for targeted vaccine delivery. ***The Journal of Immunology*****, 2014, 192: 4697–4708.**

Mouse CD8α$^+$ myeloid dendritic cells (mDC) respond strongly to TLR3 ligands and excel at CD8$^+$ T lymphocyte cross-priming, as compared with the other DC subsets, conventional mDC, and plasmacytoid DC (pDC) (1–3). CD8α$^+$ mDC express high levels of molecules involved in cellular Ag uptake, virus recognition, or cross-talk with CD8 T cells, altogether promoting cross-presentation to CD8$^+$ T lymphocytes. These molecules include CD205 (lectin mediating phagocytosis and CpG uptake) (4), CLEC9a (C-type lectin involved in the uptake of apoptotic/necrotic cells) (5), cell adhesion molecule 1 (CADM1), which mediates adhesion to activated CD8$^+$ T lymphocytes and NK cells (6–10), and TLR3 (that recognizes virus-derived dsRNA and is triggered by the polyinosinic-polycytidylic acid [poly(I:C)] adjuvant) (11). An equivalent DC subset has been identified by comparative genomic analysis and functional studies in human CD141(BDCA-3)$^+$ mDC and sheep SIRPα^{neg}CD26$^+$ mDC (3, 6, 7, 11–15). Human CD141$^+$ mDC also express high levels of CD162 (P-selectin glycoprotein ligand-1) (8) and have a strong capacity to cross-present, but not with the same exclusivity as what is claimed for murine CD8α$^+$ mDC (16, 17), at least at steady state (18). The chemokine receptor XCR1 is a specific and conserved marker for sheep SIRPα^{neg}CD26$^+$, mouse CD8α$^+$, and human CD141$^+$ mDC and has been proposed to promote their functional interactions with CD8$^+$ T lymphocytes

*INSERM Unité 1016, Institut Cochin, 75014 Paris, France; †Centre National de la Recherche Scientifique Unité Mixte de Recherche 8104, 75014 Paris, France; ‡Université Paris Descartes, 75006 Paris, France; §K.G. Jebsen Center for Research on Influenza Vaccines, Oslo University Hospital, University of Oslo, 0027 Oslo, Norway; ¶Center for Immune Regulation, Institute of Immunology, Oslo University Hospital Rikshospitalet, University of Oslo, 0424 Oslo, Norway; ‖Centre d'Immunologie Marseille-Luminy, Université de la Méditerranée, 13288 Marseille, France; #INSERM, Unité 631, 13288 Marseille, France; **Centre National de la Recherche Scientifique, Unité Mixte de Recherche 6102, 13288 Marseille, France; and ††Assistance Publique-Hôpitaux de Paris, Hôpital Cochin, 75014 Paris, France

[1]Current address: Program in Emerging Infectious Disease, Duke–National University of Singapore Graduate Medical School, Singapore.

[2]J.-P.J. and M.R. contributed equally to this work.

[3]R.C. and A.H. contributed equally to this work.

Received for publication September 12, 2013. Accepted for publication March 13, 2014.

This work was supported by INSERM, a Centre National de la Recherche Scientifique–Assistance Publique-Hôpitaux de Paris collaboration, the Université Paris Descartes, the Agence Nationale de Recherches sur le SIDA et les hépatites virale, the French Government's Investissement d'Avenir program, Laboratoire d'Excellence "Integrative Biology of Emerging Infectious Diseases" Grant ANR-10-LABX-62-IBEID, and a Université Paris Diderot doctoral fellowship (to S.A.). C.-A.D. was the recipient of an Agence Nationale de Recherches sur le SIDA et les hépatites virales fellowship.

C.-A.D., M.D., V.F., R.C., and A.H. designed the experiments; C.-A.D., J.-P.J., M.R., S.A., C.S., and V.F. conducted the experiments; M.D., R.C., and A.H. conceived the subject and gathered funding; E.F. and B.B. provided vaccibodies and methods to use them; C.-A.D., J.-P.J., M.R., and V.F. conducted data analyses; C.-A.D., J.-P.J., M.R., V.F., R.C., and A.H. interpreted the data and wrote the manuscript; all authors contributed to writing of the manuscript; R.C. and A.H. supervised the project.

Address correspondence and reprint requests to Anne Hosmalin, Institut Cochin, INSERM Unité 1016, Centre National de la Recherche Scientifique Unité Mixte de Recherche 8104, Université Paris Descartes, Batiment Gustave Roussy, 27 Rue du Faubourg Saint Jacques, 75014 Paris, France. E-mail address: anne.hosmalin@inserm.fr

The online version of this article contains supplemental material.

Abbreviations used in this article: *B2M*, β$_2$-microglobulin; CADM1, cell adhesion molecule 1; DC, dendritic cell; FMO, fluorescence-minus-one; HPRT, hypoxanthine phosphoribosyl transferase; lin, lineage; mDC, myeloid DC; MFI, mean fluorescence intensity; MHC-II, MHC class II; pDC, plasmacytoid DC; poly(I:C), polyinosinic-polycytidylic acid; pVL, plasma viral load; SMC, spleen mononuclear cell.

www.jimmunol.org/cgi/doi/10.4049/jimmunol.1302448

and NK cells. Vaccination strategies targeting CLEC9a (19) or CD205 have shown promising results in mice (20) and humanized mice (21) and are currently considered for translation into humans. Nonhuman primates, and particularly macaques, are privileged animal models for such preclinical vaccinal studies. Although CD205 targeting has been shown to be immunogenic in macaques (22), studies in humans have demonstrated that CD205 is quite promiscuously expressed in primates (23). Other receptors would therefore be better suited for selective targeting in primates. Further complicating the matter, equivalent cells have not yet been identified in primates. Therefore, we designed a strategy based on our previous work comparing sheep, mouse, and human DC subsets. We reasoned that macaque DC equivalent to sheep SIRPα^{neg} CD26$^+$, mouse CD8α$^+$, and human CD141$^+$ mDC should express the same conserved membrane markers, share the same transcriptomic signature, and be highly reactive to TLR3 triggering. Indeed, we were able to: 1) identify lineage (lin)^{neg} XCR1$^+$ mDC in rhesus macaques using polychromatic flow cytometric labeling with Abs and fluorochrome-labeled XCL1; 2) confirm by real-time PCR the expression pattern of all of the genes tested as compared with other macaque myeloid cells; and 3) demonstrate their unique high reactivity to TLR3 triggering for TNF-α production and CD40 upregulation. Hence, for the first time, to the best of our knowledge, we rigorously identified the macaque DC homologous to mouse CD8α$^+$ and human CD141$^+$ professional cross-presenting mDC.

Identification of the equivalent of murine CD8α$^+$ mDC in macaques is important for vaccination. Indeed, cross-presentation is required for presentation to cytotoxic CD8$^+$ T lymphocytes of Ag sources other than live viruses. Live attenuated viruses cannot be used for vaccination against many pathogens. For instance, in SIV$_{mac251}$ infection, the best animal model for HIV-1 infection, the most protective vaccinal viruses can revert to pathogenic strains (24).

To illustrate the importance of our new myeloid subset definition, we tested the variations of dendritic and monocytic subsets in SIV$_{mac251}$ infection, the most relevant animal model for pathogenic HIV-1 infection. A prophylactic or therapeutic vaccine against HIV is needed to prevent pathogenic infection or induce immune response recovery during infection, in conjunction with antiretroviral treatments (which cannot be interrupted without viral replication resumption). HIV-1 infection induces CD4$^+$ T lymphocyte depletion and AIDS. It induces mDC and pDC depletion, at least in patients with high viral loads (25–34). Among DC subsets, CD141$^+$ mDC show the deepest attrition (35). Conversely, CD14$^{+/-}$CD16^{++} nonclassical monocytes (36, 37) accumulate in the blood from viremic or AIDS patients (38–40). SIV$_{mac251}$ infection induces similar variations as HIV-1 infection for pDC (41–43). In animals with progressive infection, mDC are depleted (44, 45), whereas in animals remaining disease free for 60 wk, their numbers increase (41, 45). CD14$^+$CD16$^+$ intermediate and CD14$^{+/-}$CD16^{++} nonclassical subsets are increased, particularly at the AIDS stage, and newly recruited and dividing monocytes/macrophages are found in SIV encephalitis lesions (46–50).

In this study, we took advantage of our novel phenotypic key to characterize unequivocally XCR1$^+$ mDC and rigorously distinguish DC and myeloid subsets in macaques. We examined how infection with a pathogenic immunodeficiency virus affects the homeostasis of DC and other myeloid cell subsets kinetically and not only in blood but also in a secondary lymphoid organ, the spleen, and how this correlates with viral burden. We found that during SIV infection, XCR1$^+$ mDC increased transiently in the circulation during the first days of acute infection and were depleted in blood and spleen during advanced disease.

Materials and Methods

Blood and spleen macaque samples and mononuclear cell isolation

Ten healthy and 17 SIV-infected rhesus macaques (*Macaca mulatta*) were studied (51) (Table I). Among healthy macaques, two (078016 and 066160) had previously received IL-7 injections >1 y prior to euthanasia. SIV$_{mac251}$ infection was performed i.v. using 50 AID50 (infectious doses per monkey). Sacrifice was performed at the acute (n = 8), chronic (n = 2), or AIDS (n = 7) stages. PBMC and spleen mononuclear cells (SMC) obtained after Ficoll Paque gradient centrifugation were frozen and conserved in liquid nitrogen, unless sorted before freezing. Research was approved by animal experimentation ethical committee Paris 1 (2008-0006, 2010-0009, and 2011-0001).

Twelve-color flow cytometric analysis using Abs and vaccibodies

The Abs used for FACS analyses and flow cytometric cell sorting were all mouse anti-human mAbs, except the chicken anti-human CADM1 IgY primary Ab and its secondary conjugate donkey anti-chicken IgY, associated with PerCP. We used the following mAbs that were all designed and validated for flow cytometry: isotype controls mouse IgG1–Pacific Blue (clone MG128; Invitrogen/Life Technologies); mouse IgG2a-FITC (clone A12689; Beckman Coulter); and mouse IgG1-allophycocyanin and mouse IgG1-PE (clone MOPC-21), both from BD Biosciences. Specific anti-human Abs that cross react with rhesus macaque molecules were: anti-human CD123-FITC (clone G155-178, 1/10), anti-human HLA-DR–PE-Cy7 (MHC class II [MHC-II]; clone L243, 1/100), anti-human CD16–APC-H7 (clone 3G8, 1/40), anti-human CD20-FITC (clone 2H7, 1/10), anti–nonhuman primate CD45-V500 (clone 2D1, 1/25), anti-human CD162-PE (clone 4DL1, 1/10), anti-human CD205-PE (clone MG38, 1/10), and anti-human CD141 (BDCA-3)–PE (clone 1A4), all from BD Biosciences; anti-human CD11c–Alexa Fluor 700 (clone 3.9, 1/10; eBioscience); anti-human CD1c (BDCA-1)–Pacific Blue (clone L161, 1/500; BioLegend); anti-human CLEC9a-APC (clone 683409, 1/40; R&D Systems); anti-human CD20-PE–Texas Red (clone HI47, 1/10), anti-human CD16–Alexa Fluor 700 (clone 3G8, 1/10), and anti-human CD14-Qdot655 (clone TüK4, 1/100) (Invitrogen/Life Technologies); chicken IgY anti-human CADM1 (clone 3E1 used at a final dilution of 1/800; MBL International); and donkey Ig anti-chicken IgY F(ab′)$_2$-PerCP (1/50 final dilution; Jackson ImmunoResearch Laboratories). Fluorescence-minus-one (FMO) controls were used to define the positivity of various molecules for the different cell subsets that could be defined with the other Abs used in our flow cytometric panel. In these FMO samples, the proper fluorochrome-conjugated isotype controls were added in place of the Ab directed against the molecule for which the limit of positivity was required. To reduce the number of FMO samples, multiple FMOs were combined within a single sample but only for Abs coupled to fluorochromes that had absolutely no spectral overlap. Therefore, a fluorescence-minus-three control sample was used in which isotype controls coupled to Pacific Blue, FITC, and allophycocyanin were combined to delineate the positivity for CD1c (Pacific Blue), CD123 (FITC), and Clec9a (allophycocyanin). We also used an FMO for PE, which was our variable channel (CD162-PE, CD205-PE, or CADM1 plus secondary Ab-PE). Concerning CD16, the limit between CD16$^-$ and CD16$^+$ monocytes was easily defined as the CD14^{++}CD16$^-$ classical subset always appeared as a round, well-defined population. The limit between nonclassical CD14$^{+/-}$CD16^{++} and intermediate CD14$^+$CD16$^+$ cells was first defined at the vertical of the classical CD14^{++}CD16$^-$ monocytes that showed the lowest CD14 expression. Following this positioning of the two CD16$^+$ monocyte subset gates, we checked also that intermediate monocytes had the highest mean fluorescence intensity (MFI) for MHC-II (defined using an anti-human HLA-DR Ab). No isotype control was used in place of the anti-CD11c Ab because this molecule was not used to define cell subsets or a percentage of positivity for CD11c. It was initially put into our multicolor panel because human mDC express CD11c, and macaque mDCs were previously thought to be CD11c$^+$.

We also used bivalent human XCL1-mCherry vaccibodies that bind human XCR1 (50 μg/ml; E. Fossum and B. Bogen, manuscript in preparation). As negative controls, we used a mutated version of XCL1 in which cystein 11 is mutated to alanine [XCL1(C11A)-mCherry; 50 μg/ml], as well as anti–NIP-mCherry (a single-chain Fv Ab binding the hapten NIP as previously described) (Supplemental Fig. 1) (52–54). Construction of the vaccibody gene construct, including cloning of the anti-NIP, has been previously described (53). Human XCL1 and XCL1(C11A) were ordered from Genscript and cloned into the vaccibody gene construct using BsmI and BsiWI. mCherry was cloned into the construct using SfiI, as previously described (55). To express the vaccibodies, the gene constructs were stably

Table I. Blood and spleen samples and clinical data from macaques

Macaque	Symbols in Fig. 5A	Age (y)	Sex	Infection Stage	Time Postinfection	$CD4^+$ T (Cells/μL)	VL (Log_{10} RNA Copies/ml)	Spleen	Blood
76144	Open circle	3	F	Uninfected	—	ND	—	Yes	Yes
78016	Open circle	4	F	Uninfected	—	ND	—	Yes	No
88282	—	4	F	Uninfected	—	ND	—	Yes	No
90358	Open circle	3	F	Uninfected	—	ND	—	Yes	Yes
66160	Open circle	5	F	Uninfected	—	ND	—	No	Yes
90528	Open circle	3	F	Uninfected	—	ND	—	No	Yes
90066	Open circle	3	F	Uninfected	—	ND	—	No	Yes
90348	Open circle	3	F	Uninfected	—	ND	—	No	Yes
90526	Open circle	3	F	Uninfected	—	ND	—	No	Yes
81998	Open circle	3	F	Uninfected	—	ND	—	No	Yes
90968	—	4	F	Uninfected	—	ND	—	No	Yes
90874	Open circle	3	F	Uninfected	—	ND	—	No	Yes
66026	Gray diamond	5	F	Acute	3 d	1043	Undetectable	Yes	No
66032	Gray diamond	5	F	Acute	3 d	262	Undetectable	Yes	Yes
97R0342	Gray diamond	12	F	Acute	3 d	517	2.31	Yes	Yes
98R0008	Gray circle	11	F	Acute	7 d	70	3.16	Yes	Yes
66036	Gray circle	5	F	Acute	7 d	224	3.48	Yes	Yes
66096	Gray square	5	F	Acute	10 d	267	5.17	Yes	Yes
66056	Gray square	5	F	Acute	10 d	718	5.32	Yes	Yes
088178	Gray triangle	5	F	Acute	14 d	533	6.59	Yes	Yes
98R0032	Gray triangle	11	F	Acute	14 d	151	7.47	Yes	Yes
98R0044	Black circle	11	F	Chronic	10 mo	ND	5.25*	Yes	No
98R0078	Black circle	11	F	Chronic	10 mo	ND	5.75*	Yes	Yes
501010	Black circle	4	F	AIDS	7.5 mo	ND	ND	Yes	Yes
503068	Black circle	5	F	AIDS	15.5 mo	ND	ND	Yes	Yes
504034	Black circle	5	F	AIDS	15.5 mo	ND	ND	Yes	Yes
98R0016	Black circle	12	F	AIDS	37 mo	ND	ND	Yes	Yes
26063	Black circle	6	F	AIDS	33 mo	ND	ND	Yes	Yes
503052	Black circle	5	F	AIDS	25 mo	ND	ND	Yes	Yes
504006	Black circle	4	F	AIDS	11 mo	ND	ND	No	Yes

*Viral load obtained 2 to 3 mo before euthanasia.
F, female.

transfected into NS0 cells, which were grown in rollerbottles. mCherry vaccibodies were purified by harvesting supernatants and applying them onto a Sepharose 4 Fast Flow column (GE Healthcare) conjugated with an anti-mCherry Ab (clone 1) (55). Eluted vaccibodies were dialyzed twice in PBS, concentrated using a 50-Kd cutoff Vivaspin column (Sartorius Stedim Biotech), aliquoted, and stored at −80°C until use.

PBMC or SMC (2.10^6 cells/tube) were thawed in the presence of 20 IU/ml DNaseI to prevent aggregates immediately before labeling. Cells were washed and incubated with Live/Dead blue dye (30 min, 4°C; Invitrogen/Life Technologies) in PBS. Then, 5% heat-inactivated human serum was added (15 min, 4°C; AbCys). Cells were labeled with Abs (PBS-2% FCS and 2 mM EDTA, 30 min, 4°C), then washed, fixed with 0.5% paraformaldehyde, and events acquired using an FACS LSRII (BD Biosciences). XCR1 labeling by vaccibodies or NIP was performed (30 min, 4°C) after Ab labeling. Events were acquired using a BD FACSAria III (BD Biosciences). Analyses were carried out using BD FACSDiva (BD Biosciences) and FlowJo (Tree Star). The median number of analyzed events for the $CADM1^+$ mDC population was 206, the minimum was 7 (for a macaque with AIDS), and the highest was 1358. Other DC and monocyte subsets were more numerous. The absolute number of cells per microliters of blood from acutely infected macaques was calculated by multiplying the hemocytometer complete blood count (performed independently on whole blood) of mononuclear cells (monocytes plus lymphocytes) to the percentage of cells among $CD45^{hi}$ events.

Flow cytometric cell sorting

Freshly isolated SMC were incubated (15 min, 4°C) with PBS-5% human serum and then labeled prior to sorting using the BD FACSAriaIII (BD Biosciences) set for high-purity sorting. Cells were labeled with the following fluorescently labeled Abs or vaccibodies: CD45-V500, CD20-FITC, HLA-DR–allophycocyanin-Cy7, CD14-Qdot655, CD16–Alexa Fluor 700, CD1c (BDCA-1)–Pacific Blue, chicken IgY anti-human CADM1 followed by a donkey Ig anti-chicken IgY F(ab')-PerCP, and human XCL1-mCherry vaccibodies, which were added concomitantly with the donkey Ig anti-chicken IgY F(ab')-PerCP secondary Ab. Purification was obtained to at least 98%.

TLR3 simulation in vitro

Freshly purified PBMC were cultured (5.10^6 cells/ml, 37°C, 5% CO_2) in RPMI 1640 plus glutamax-10% FCS, with 5 or 20 μg/ml poly(I:C) (Invitrogen) or 100 ng/ml LPS (Sigma-Aldrich) in polypropylene tubes. For TNF-α intracellular FACS analyses, cells were cultured for 5 h, and brefeldin A (10 μg/ml; Sigma-Aldrich) was added during the last 4 h. For CD40 expression, cells were cultured for 18 h and labeled as above with addition of anti–CD40-APC clone 5C3 (1/10; BD Biosciences). For intracellular TNF-α detection, following membrane labeling as above without anti-CD11c, cells were fixed, permeabilized (BD Cytofix/Cytoperm kit; BD Biosciences), and incubated with anti–TNF-α–Alexa Fluor 700 clone MAB11 (1/10, BD Biosciences; 45 min, 4°C) in Perm/Wash buffer.

Real-time RT-PCR quantitative analysis of transcript expression by sorted cellular subsets

Purified cell populations were lyzed in 350 μl RLT buffer (Qiagen) containing 1% of 2-ME (Sigma-Aldrich) and stored at −80°C. Total mRNA were purified using the RNeasy kit (Qiagen), according to the manufacturer's instructions: briefly, lysates were homogenized using QIAshredder (Qiagen), and residual DNA was removed by on-column DNase digestion using the RNase-Free DNase Set (Qiagen). mRNA were eluted using 2 × 40 μl RNase-free water and immediately subjected to a reverse transcription step with the QuantiTect Reverse Transcription Kit (Qiagen). cDNA were kept at −20°C.

Primers specific for each of 12 specific genes (*CLEC9A*, *RAB7B*, *TLR3*, *BATF3*, *XCR1*, *CLEC4C*, *ILT7*, *TLR7*, *TLR9*, *CD1E*, *TLR4*, and *TLR8*) and 4 housekeeping genes (hypoxanthine phosphoribosyl transferase [*HPRT*], *GAPDH*, β-actin [*ACTB*], and β_2-microglobulin [*B2M*]) were defined on macaque cDNA sequences (accession numbers NM_001194664.1, XM_001082679.2, NM_001036685.1, XM_001107737.2, XM_001114298.1, XM_002798473.1, XM_001083251.2, NM_001130426.1, NM_001130431.1, NM_001042658.1, NM_001037092.1, and NM_001130427.1, respectively; Table II). To detect small amounts of DNA from low numbers of FACS-sorted cells, we developed a specific nested PCR assay as currently performed in our laboratory (56, 57). cDNA were first PCR amplified (final volume 50 μl, 15 min initial denaturation at 95°C, then 25 cycles of 30 s at 95°C, 30 s at 60°C, and 3 min at 72°C). To decrease the amount of RNA necessary for this analysis and thus to increase the number of sequences that can be quantified, multiplex PCR amplifications were designed to measure in the same round: 1) *CLEC9A* and *BATF3*; 2) *TLR7* and *TLR9*; 3) *TLR4* and *TLR8*; and 4) *HPRT*,

GAPDH, *ACTB*, and *B2M*. The number of cycles (25) for this first amplification step was adjusted to ensure that all amplifications remained in the exponential phase of the reaction. PCR products were quantified using LightCycler 480 Real-Time PCR Technology with LightCycler 480 SYBR Green I Master Mix (Roche Applied Science), performed on 1/190th of the initial PCR products: 10 min initial denaturation at 95°C, followed by 45 cycles of 10 s at 95°C, 10 s at 64°C, and 15 s at 72°C. The 16 genes were quantified in duplicate for the 8 purified cell populations. Results are displayed for each gene in each population as fold differences compared with the most weakly expressed housekeeping gene, HPRT, using the 2eΔCp method (ΔCp corresponding to the number of amplification cycles between the detectability of HPRT amplicons and that of the studied gene).

Statistical analysis

Results are given as medians. Mann–Whitney *U* test was used to compare controls and infected groups and Wilcoxon rank-sum test was used to compare cell subsets (Fig. 2). Correlations were evaluated by Spearman test. Differences were defined as statistically significant when $p < 0.05$. The p values were shown when < 0.15. All these nonparametric tests were performed using GraphPad Prism 5 (GraphPad).

Results

Definition of a simian mDC subset phenotypically homologous to human XCR1$^+$ CD141 (BDCA-3)$^+$ DC

To study all DC and monocyte subsets simultaneously in macaques, we carried out 12-color flow cytometric analysis. PBMC from nine healthy macaques were studied. The gating strategy is shown for a representative uninfected macaque (monocyte and DC subsets outlined in red, Fig. 1A). In these analyses, among live (Live/Dead$^-$) singlet (side scatter width/side scatter area and forward light scatter height/forward light scatter area dot plots) CD45$^+$ cells, MHC-II$^+$CD20$^+$ B lymphocytes, monocyte subsets (classical CD14^{++}CD16$^-$, intermediate CD14$^+$CD16$^+$, and nonclassical CD14$^{+/-}$CD16^{++}) (Table II), and lin^{neg} MHC-II^{lo}CD123$^+$ pDC were simultaneously defined. Among MHC-II$^+$ lin^{neg} (CD20$^-$ CD14$^-$CD16$^-$) cells, concomitant detection of CD1c, CADM1, and CD205 allowed us to distinguish the previously described CD1c$^+$ mDC from the yet overlooked CADM1$^+$CD205^{hi} mDC (Fig. 1A). CADM1$^+$ mDC also strongly expressed CD162-like human CD141$^+$ mDC. However, CADM1$^+$ mDC expressed CLEC9A only in 2 out of 27 tested macaques. FACS analysis was carried out on human PBMC using the same Abs with the addition of anti-CD141 (Fig. 1B). Among lin^{neg} MHC-II(HLA-DR)$^+$ cells, we defined CD1c$^+$ mDC (beige subset) and CD141$^+$ mDC (red subset) (Fig. 1B). The latter had the same phenotype as macaque CADM1$^+$ mDC (lin^{neg}MHC-II$^+$CADM1$^+$CD205^{hi}CD162^{hi}), as previously described for human CD141$^+$ mDC and/or mouse CD8α$^+$ mDC (8, 11, 14, 58). The MFIs of CADM1, CD205, and MHC-II on different subsets were evaluated in the blood from the nine uninfected macaques (Fig. 2A). CADM1$^+$ mDC had the highest CADM1 and CD205 expression levels ($p < 0.004$), compared with all subsets, and a lower MHC-II expression as compared with CD1c$^+$ mDC, just like human CD141$^+$ mDC (Fig. 2A). Using mCherry-coupled XCL1 (52), we observed that like human CD141$^+$ mDC and murine CD8α$^+$ mDC, macaque CADM1$^+$ mDC were the only cells expressing XCR1 (Fig. 1C) (7, 14, 52). Binding of mCherry-coupled human XCL1 to macaque CADM1$^+$ mDC (MFI 1619) was specific compared with nonspecific NIP-mCherry binding (MFI 337), and it was strongly reduced (MFI 439) by the XCL1(C11A) mutation (Fig. 1C, Table III). The highest XCR1 expression level by CADM1$^+$ mDC as compared with all the other cell subsets was confirmed using PBMC and SMC from six different macaques (PBMC, $n = 4$; SMC, $n = 2$; MFI for CADM1$^+$ mDC median: 1415; SEM: 85.9; for CD14$^{+/-}$CD16^{++} monocytes, median: 361.0, SEM: 67.2; $p = 0.002$; Fig. 2B). As controls, the MFIs of mutant XCL1 (C11A) and irrelevant NIP binding were not significantly increased in CADM1$^+$ mDC as compared with the other cell subsets [XCL1(C11A) MFI for CADM1$^+$ mDC median: 351.5, SEM: 90.0; for CD14$^{+/-}$CD16^{++} monocytes, median: 146.0, SEM: 59.4, $p > 0.20$; NIP MFI for CADM1$^+$ mDC median: 329.0, SEM: 60.1; for CD14$^{+/-}$CD16^{++} monocytes, median: 184.5, SEM: 24.2] (Fig. 2B).

Therefore, as in our previous comparative studies, XCR1 was again a key molecule in specifically identifying this mDC subset in macaques. Consequently, the XCR1$^+$ DC nomenclature will be used through this report. In the absence of specific anti-simian XCR1 Abs, CADM1 or CD205 Abs were also used to distinguish these cells from conventional CD1c$^+$ DC.

The median proportion of circulating XCR1$^+$ DC characterized as in Fig. 1 was 0.06% (range 0.04–0.09%; SEM 0.007; $n = 9$). XCR1$^+$ DC were also characterized in the spleens from three healthy macaques using a similar gating strategy (Supplemental Fig. 2), and their median proportion among CD45$^+$ mononuclear cells was 0.14 (0.08–0.39%; SEM: 0.09; $n = 3$).

High CD11c expression is characteristic of CD16$^+$ monocytes and not of mDC in macaques

Most previous studies of mDC during SIV infection in macaque defined them like in humans as lin^{neg}MHC-II$^+$CD11c$^+$ but without an anti-CD16 Ab in the lineage mixture (41, 45). We confirmed the observation by Autissier et al. (59) that CD1c$^+$ mDC only weakly express CD11c, therefore most CD20$^-$CD14$^-$ MHC-II$^+$CD11c$^+$ cells correspond to CD16$^+$ monocytes, and the population expressing the highest levels of CD11c corresponds to nonclassical CD14$^{+/-}$CD16^{++} monocytes (Fig. 1D, Supplemental Fig. 3).

Simian XCR1$^+$ DC displayed the same molecular signature as in humans and mice

We next evaluated, in FACS-sorted spleen lin(CD14/CD16/CD20)$^-$MHC-II$^+$CADM1$^+$XCL1$^+$ mDC, CD1c$^+$ mDC, lin$^-$ MHC-II^{lo}CD123$^+$ pDC, and classical CD14^{++}CD16$^-$ monocytes from two uninfected macaques, the expression level of genes known to be strongly expressed either in human and murine XCR1$^+$ mDC homologs or in human pDC, CD1c$^+$ mDC, and monocytes (7, 13, 14, 52) (Fig. 3, Supplemental Fig. 2). As a control, we checked that all of the housekeeping genes tested had a similar expression level in all cellular subsets (Fig. 3D). We confirmed at the RNA level that, like in humans or mice, simian XCR1$^+$ mDC expressed the highest levels of the genes encoding XCR1, CLEC9A, and TLR3, the transcription factor BATF3, and the small GTPase RAB7B (Fig. 3A). *CLEC9A* mRNA was strongly expressed in both macaques studied, in contrast to the failure of surface labeling using anti-human CLEC9A Ab in most macaques including these two macaques (staining of XCR1$^+$ mDC with anti-human CLEC9A Ab in only 2 other macaques out of the 28 macaques studied). This suggested a polymorphism in the macaque CLEC9A molecule affecting the epitope recognized by the anti-human CLEC9A Ab. Therefore, this Ab is not suitable to label XCR1$^+$ DC in rhesus macaques.

In agreement with data in humans, the *CLEC4C*, *ILT7*, *TLR7*, and *TLR9* genes were all expressed at higher levels in FACS-sorted macaque pDC (Fig. 3B), whereas *CD1E*, *TLR4*, and *TLR8* were strongly expressed by FACS-sorted CD14^{++}CD16$^-$ monocytes, and to a lesser extent by CD1c$^+$ mDC, from the two uninfected macaques tested (Fig. 3C). Therefore, XCR1$^+$ DC displayed the same specific molecular signature in rhesus macaques as in humans or mice.

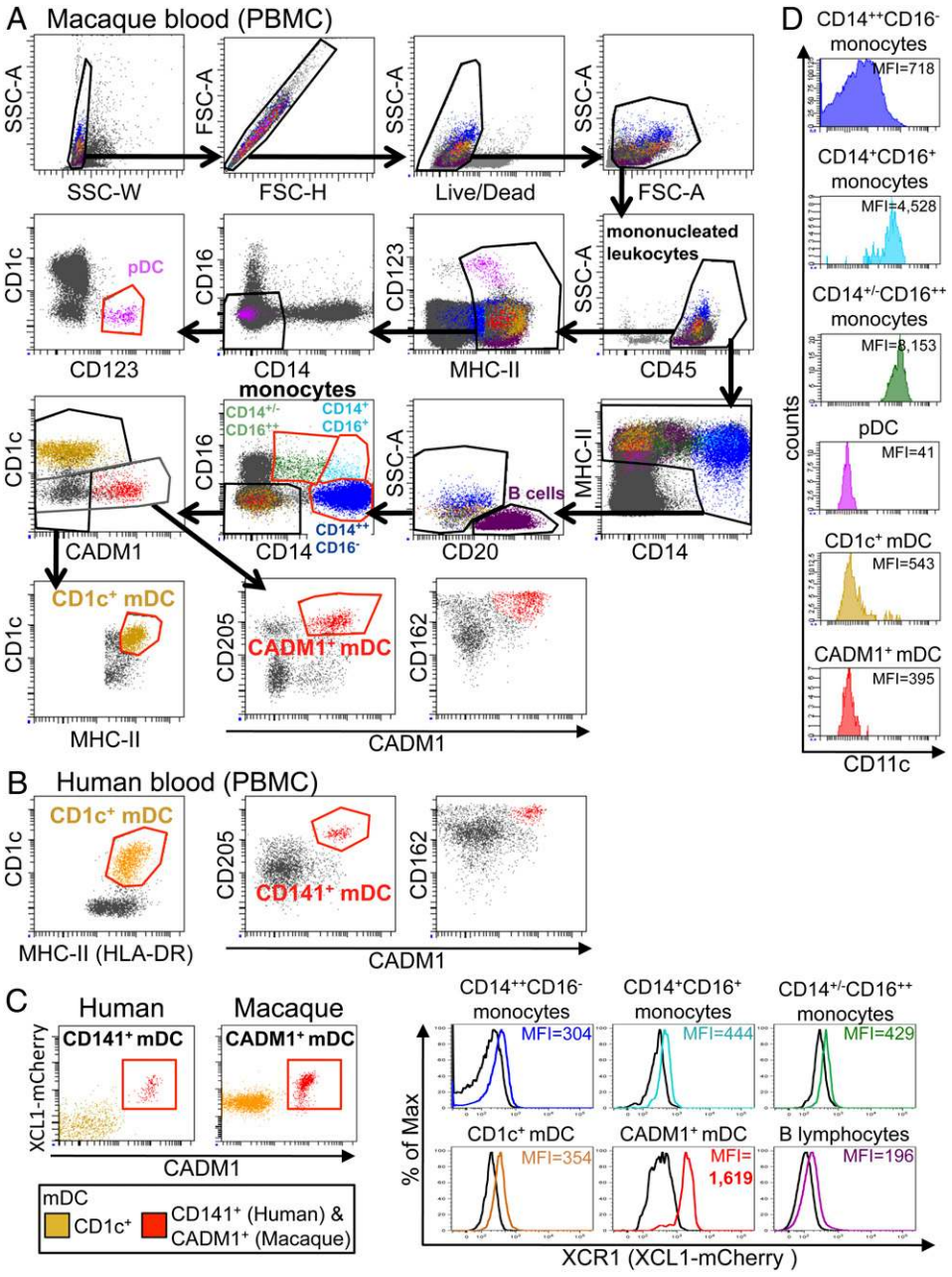

FIGURE 1. Flow cytometric characterization of a macaque mDC subset phenotypically homologous to human XCR1$^+$CD141$^+$ mDC. (**A**) The gating strategy to analyze B cells, monocyte, and DC subsets among PBMC from an uninfected macaque by 12-color flow cytometry is shown. CD162 expression by CADM1$^+$ mDC is also shown. (**B**) Human PBMC labeled with the same Abs and for CD141, analyzed as in (A). (**C**) Flow cytometric dot plots showing CADM1 versus XCR1 expression (using mCherry-coupled XCL1) by human CD141$^+$ and macaque CADM1$^+$ mDC (red) and by human and macaque CD1c$^+$ mDC (beige). Histograms show the binding of XCL1 (colored histograms) or mutant XCL1 (C11A) (black histograms) by macaque monocyte and mDC subsets compared with B lymphocytes used as negative controls (XCR1 MFI indicated in each histogram). (**D**) CD11c expression by macaque monocytes and DC defined in (A). CD11c MFI is indicated in each histogram. FSC-A, forward light scatter area; FSC-H, forward light scatter height; SSC-A, side scatter area; SSC-W, side scatter width.

Simian XCR1$^+$ mDC had stronger responses to TLR3 stimulation than the other APCs

To assess whether simian XCR1$^+$ mDC were functionally homologous to human and mouse XCR1$^+$ mDC, we evaluated whether they had stronger responses to TLR3 triggering than other mDC or DC populations. Freshly purified PBMC from healthy macaques were stimulated using the TLR3 agonist poly(I:C) or, as a control, the TLR4 agonist LPS. TNF-α production was quantified by intracellular FACS analysis in XCR1$^+$ (defined in this study as CADM1$^+$) or CD1c$^+$ mDC, pDC, and CD14^{hi} or CD14^{lo} monocytes, as well as in B lymphocytes, which do not express TLR3 (60) (Fig. 4). Representative results are shown for the different cell subsets from one macaque (Fig. 4A). A strong TNF-α production was detected following poly(I:C) stimulation only in CADM1$^+$ mDC in response to 5 μg/ml (CADM1$^+$ mDC versus pDC or CD14^{lo} monocytes, $p = 0.008$; versus B lymphocytes and CD14^{hi} monocytes, $p = 0.012$; and versus CD1c mDC, $p = 0.016$) or 20 μg/ml (CADM1$^+$ mDC versus CD1c$^+$ mDC, pDC, CD14^{lo}, and CD14^{hi} monocytes, $p = 0.008$; and versus B lymphocytes, $p = 0.012$). As a positive control, monocytes had the highest response to LPS (CD14^{lo} and CD14^{hi} monocytes versus all other subsets, $p = 0.008$) (Fig. 4B, 4C). Comparatively, CADM1$^+$ mDC responded weakly to LPS (8.3% TNF-α–positive cells), consistently with their low expression of TLR4. The MFI of CD40 was increased 2.4-fold ($p = 0.1$ using the nonparametric Mann–Whitney U test) on CADM1$^+$ mDC and only 1.9-fold on CD1c$^+$ mDC ($p = 0.2$), and it was not increased in B lymphocytes, pDC, CD14^{hi}, or CD14^{lo} monocytes ($p > 0.4$) ($n = 3$, Fig. 4B, 4D). Thus, XCR1$^+$ mDC had a stronger cytokine response to TLR3 stimulation than the other APCs in macaques, as in humans or mice.

High circulating XCR1$^+$ mDC counts during acute SIV infection, but depletion during AIDS

The SIV infection model makes it possible to evaluate immunological parameters at all stages of the infection, particularly during the first days following infection, which are nearly impossible to

Table II. Primers used for real-time PCR on FACS-sorted DC subsets and CD14^{++}CD16$^-$ monocytes

Gene Name	5′ Out Primer	3′ Out Primer	5′ In Primer	3′ In Primer
CLEC9A	TACACCTCTCTTCAGTGGGA	CAGCGTGGAACCTTCCTTTA	AGGAGCATGGTGTCTTGTGA	GACTGCAGTTATGGGCTGAA
RAB7B	ATGAATCCCCGGAAGAAGGT	TCTCTCTACACCAGCCTTGA	AGCCATTGGTGTGGGAAAGA	TTGAGCTACTTCCTGGGGTA
TLR3	CTGTCCCACTCAATCCAGAA	GTGGAAGCCAAGCAAAGGAA	CTGTCCCACTCAATCCAGAA	CAGATTCCGAACGCTTGTGT
BATF3	CCTGAGGATGATGACAGGAA	GGTGCCCCCTGTATACAATT	GAGTTGCTGCTCAGAGAAGT	GAAACCCTTCCTCCCTGGTAT
XCR1	TGTGGGTCCTGGTGAAGTAT	GAAGAGGTTGTGCTGGTAGA	TGTGGGTCCTGGTGAAGTAT	AAGACGGCGTCGAGGATGGA
CLEC4C	TCAAGCGGCTGTCCAAGTTA	ACCTGAGTGCCAGAATGTGA	TCAAGCGCTGTCCAAGTTA	TCTGACAGCCCCAGAAAA
ILT7	CAGGACTACCGTCTGGATAA	CACGTACGGGGTGTTGTTTT	CTCCATCCCATCCATGATGT	AACGTACCCCTGTTGCTGAA
TLR7	CCTAAAACTCTGCCCTGTGA	CTCAAGGCTGAGAAGCTGTA	CCTGTGATGTCACTCTGGAT	CGGTATCTCTAGAAGCTGGT
TLR9	ACCAACATCCTGGTGCTAGA	CATTCAGCCAGGAGAGAGAA	ACCAACATCCTGGTGCTAGA	GCTGAAGGTATCGGGATGTA
CD1E	TTGTGTGCCATGTCTCAGGA	GAGAGTTGGTTTAGGCGTGT	ATGTCTCAGGATTCTACCCAAA	GTTTAGGCGTGTCTTCCACT
TLR4	GAACTGCAGGTGCTGGATTT	CTAAACCAGCCAGACCTTGA	AGGAAACCCCATCCAGAGTT	TATAGGGTTCAGGGACAGGT
TLR8	CCCAAACGGTGGGCAAATAT	GCAGTTCCAGGCCAAATAGA	TGACAGAACTAGACTTGTCTGA	AGTCTTGAAATGCCCTCTTTAGT
HPRT	CTGAACGTCTTGCTCGAGAT	CGACCTTGACCATCTTTGGA	CACATTGTAGCCCTCTGTGT	CTGACCAAGGAAAGCAAAGT
GAPDH	AGGTCGGAGTCAACGGATTT	CTGACGATCTTGAGGCTGTT	GTCACCAGGGCTGCTTTTAA	GGCAGAGATGATGACCCTTTT
ACT	AGAGAGGCATTCTCACCCTGAA	CTCGTTGCCAATGGTGATGA	AACTGGGACGACATGGAGAA	CATGAGGTAGTCAGTCAGGT
B2M	GCTATCCAGCGTACTCCAAA	TTACATGTCTCGATCCCACTTA	CTCCAAAGATTCAGGTTTACTCA	TGACAAAGTCACATGGTTCACA

study in humans, and simultaneously in the circulation and lymphoid organs. In macaques sacrificed during acute SIV$_{mac251}$ infection (Table I), we measured the percentages among PBMC and CD45$^+$ SMC of all DC and monocyte subsets (as defined in Fig. 1). In the blood, XCR1$^+$ (defined in this study as CADM1$^+$), mDC proportions peaked at day 7 postinfection (gray circles, median: 0.42%; fold change as compared with uninfected macaques: 7.2) and were significantly increased in macaques tested during very early infection (day 3 plus day 7) compared with uninfected macaques (median: 0.27 versus 0.06%; $p = 0.003$, Fig. 5A). As previously described (42, 43), this was also the case for pDC (medians: uninfected, 0.09%; infected day 3 plus day 7, 0.27%; $p = 0.006$). The proportions of classical CD14^{++}CD16$^-$ monocytes (medians: uninfected, 2.57%; infected day 3 plus day 7, 8.07%; infected day 10 plus day 14, 6.71%; uninfected versus all acutely infected: $p = 0.02$), intermediate CD14$^+$CD16$^+$ monocytes (medians: uninfected, 0.07%; infected day 3 plus day 7, 0.28%; infected day 10 plus day 14, 0.49%; uninfected versus all acutely infected: $p = 0.004$), and CD1c$^+$ mDC (medians: uninfected, 0.29%; infected day 3 plus day 7, 0.75%; infected day 10 plus day 14, 0.51%) were also increased transiently but for a longer period of time during acute infection (days 3–14). In the spleen, only three uninfected macaques were analyzed, making it difficult to reach significant differences (Fig. 5A). Plasma viral loads (pVL) increased over time with maximal values around day 10 postinfection, as expected. Absolute cell counts were studied in eight acutely infected macaques to assess correlations with viral loads (Fig. 5B). Interestingly, among all cellular subsets studied, only circulating XCR1$^+$ mDC absolute counts (Spearman $r = -0.90$; $p = 0.005$) and proportions (Spearman $r = -0.81$; $p = 0.02$) showed an inverse correlation with pVL (Fig. 5B). This was not the case in the spleen.

We then measured the proportions of DC and monocyte subsets in macaques with advanced infection (two with chronic infection and pVL >5 log, seven with AIDS; Fig. 5A, Table I) compared with uninfected macaques. The proportions of XCR1$^+$ mDC among CD45$^+$ cells from the macaques with advanced infection were reduced by 5.19 in the spleens (median uninfected: 0.14% and advanced infection: 0.03; $p = 0.02$) and tended to be reduced by 2.71-fold in the blood (median uninfected: 0.06% and advanced infection: 0.02; $p = 0.05$), whereas CD1c$^+$ mDC proportions were reduced by 1.81-fold in the blood only (median uninfected: 0.29% and advanced infection: 0.16; $p = 0.04$). In contrast, pDC and monocyte subset proportions were not significantly affected by infection, both in blood and spleen. To overcome the impact of CD4$^+$ T lymphocyte depletion on DC and monocytes, we analyzed the proportions of mDC and monocyte subsets among total myeloid mononuclear cells (Fig. 5C). This highlighted a reduction in the proportions of XCR1$^+$ and CD1c$^+$ mDC among myeloid cells, especially in the blood, in macaques with advanced disease.

Therefore, SIV$_{mac251}$ infection had a clear impact on XCR1$^+$ mDC homeostasis from an early rise in the circulation to an apparently global depletion during chronic infection or AIDS.

Discussion

Cross-species transcriptomic, phenotypic, and functional comparison allowed the identification in rhesus macaques of a DC population homologous to human CD141$^+$, murine CD8α^+, and sheep CD26$^+$ mDC, XCR1 being a specific and conserved marker spanning all of these species. In addition, we show that these cells had increased circulating numbers during the first week of SIV infection in inverse correlation with viral loads and, conversely, reduced during advanced infection.

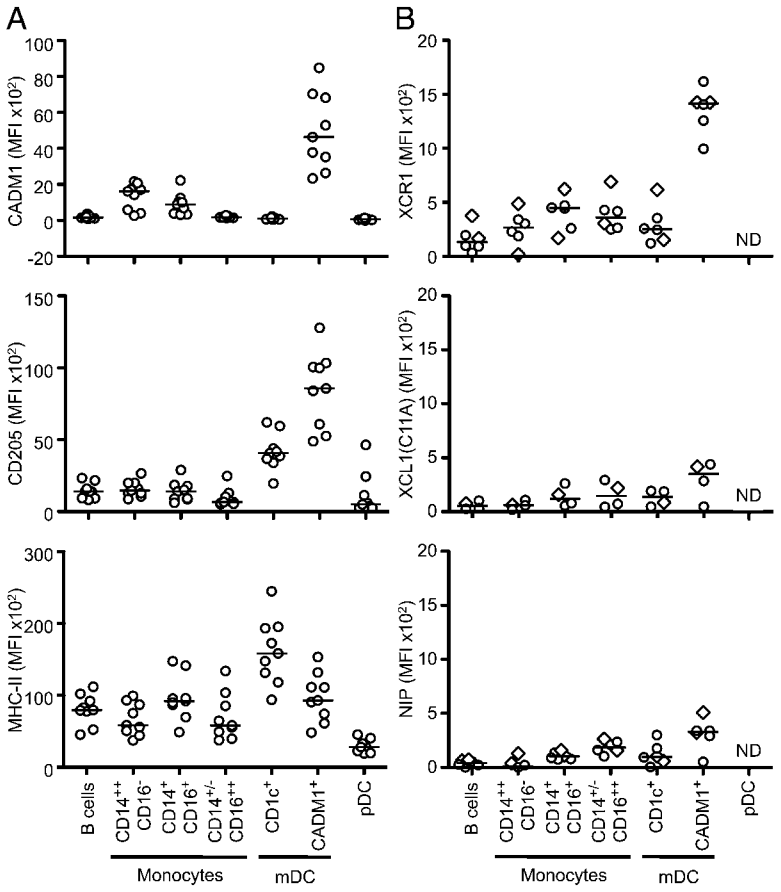

FIGURE 2. Expression levels of CADM1, CD205, MHC-II, and XCR1 molecules at the surface of different cell populations in rhesus macaques. (**A**) Graphical representation of the MFIs of CADM1, CD205, and MHC-II labeling on $CD20^+$ B lymphocytes, $CD14^{++}CD16^-$, $CD14^+CD16^+$, or $CD14^{+/-}CD16^{++}$ monocytes, $CD1c^+$ and $CADM1^+$ mDC, and pDC in the blood from nine uninfected macaques. (**B**) mCherry MFIs for $CD20^+$ B lymphocytes, $CD14^{++}CD16^-$, $CD14^+CD16^+$, or $CD14^{+/-}CD16^{++}$ monocytes, and $CD1c^+$ and $CADM1^+$ mDC isolated from the blood (open circles) or spleens (open diamonds) from different macaques stained with mCherry-coupled XCL1 [PBMC, $n = 2$; SMC, $n = 2$ (*top panel*)], mutant XCR1 (C11a) [PBMC, $n = 1$; SMC, $n = 1$ (*middle panel*)], or nonspecific [PBMC, $n = 1$; SMC, $n = 1$ (*bottom panel*)] are shown. MFIs were from the entire population, as depicted in Fig. 1C for XCR1 labeling.

For the identification of the macaque mDC population homologous to mouse $CD8\alpha^+$ and human $CD141^+$ mDC, CADM1 was found to be the cell-surface marker with the best combination of selectivity, expression reproducibility, and commercial reagent accessibility (3, 6, 7, 11, 12, 15). CADM1 binds to the class I–restricted T cell–associated molecule, a surface receptor primarily expressed on activated cytotoxic lymphocytes (8). This is thought to participate in the cross talk between $XCR1^+$ mDC and activated $CD8^+$ T lymphocytes. None of the commercial anti-human XCR1 Abs could label specifically XCR1 in our hands, even on human primary $CD141^+$ DC. However, we labeled very reproducibly and specifically macaque $XCR1^+CADM1^+$ cells using custom-made fluorescently coupled recombinant human XCL1, the ligand for XCR1, as previously performed in mice using labeled mouse XCL1 (52). Labeling was specific, as assessed using mutant molecules, and exclusive for this cell subset among mononuclear cells. Conversely, CD141 was expressed by macaque $XCR1^+$ mDC, but also by $CD1c^+$ mDC and all monocyte subsets (59), and therefore is not as distinctive of this cell subset as in humans. In addition, CLEC9A, which is expressed at the surface of human and mouse $XCR1^+$ mDC and allows them to bind necrotic cells and cross-prime their Ags to naive $CD8^+$ T lymphocytes (61), was labeled using anti-human Abs in only 2 of the 28 macaques analyzed for CLEC9A expression by flow cytometry. However, CLEC9A mRNA was specifically and highly expressed by $XCR1^+$ mDC in the two macaques analyzed for RNA expression, these two macaques being both negative for CLEC9A by flow cytometry. This suggests an interesting polymorphism in the simian CLEC9A molecule affecting the epitope recognized by the anti-human CLEC9A Ab, which therefore is not suitable to identify $XCR1^+$ DC in macaques. Hence, XCR1 seems currently to be the only cell-surface conserved specific marker in sheep, mice, macaques, and humans, and commercial Abs will be needed, but CADM1 or CD205 Abs can also be used to distinguish these cells from conventional $CD1c^+$ DC.

Table III. MFI of mCherry coupled NIP, mutant XCL1(C11A), and XCL1 at the surface of monocyte and mDC subsets defined in Fig. 1D

mCherry MFI	NIP	XCL1(C11A)	XCL1
$CD14^{++}CD16^-$ monocyte	−10	107	304
$CD14^+CD16^+$ monocyte	135	263	444
$CD14^{+/-}CD16^{++}$ monocyte	160	294	429
$CD1c^+$ mDC	93	193	354
$CADM1^+$ mDC	337	439	1619
B lymphocytes	55	103	196

The strong coexpression of CADM1, CD162, CD205, and XCR1, in combination with quantitative analysis of genes specific for the different myeloid and DC subsets, confirmed the homology among simian, human, and murine $XCR1^+$ mDC. Particularly, in the three species, these cells expressed selectively high levels of the transcription factor Batf3, which specifically drives the development of $XCR1^+$ mouse ($CD8\alpha^+$) and human ($CD141^+$) mDC at steady state (1, 62). Macaque $XCR1^+$ mDC strongly expressed the *TLR3* gene and strongly responded to the TLR3 ligand poly(I:C) by producing TNF-α and upregulating CD40, whereas all of the other APCs responded weakly or not. $XCR1^+$ mDC also strongly expressed genes encoding proteins involved in cross presentation, including CLEC9A and the small GTPase RAB7B, which is essential for the retrograde transport from endosomes to the *trans*-Golgi network, and has been hypothesized to promote assembly of the machinery required for cross presentation (52). Further functional studies

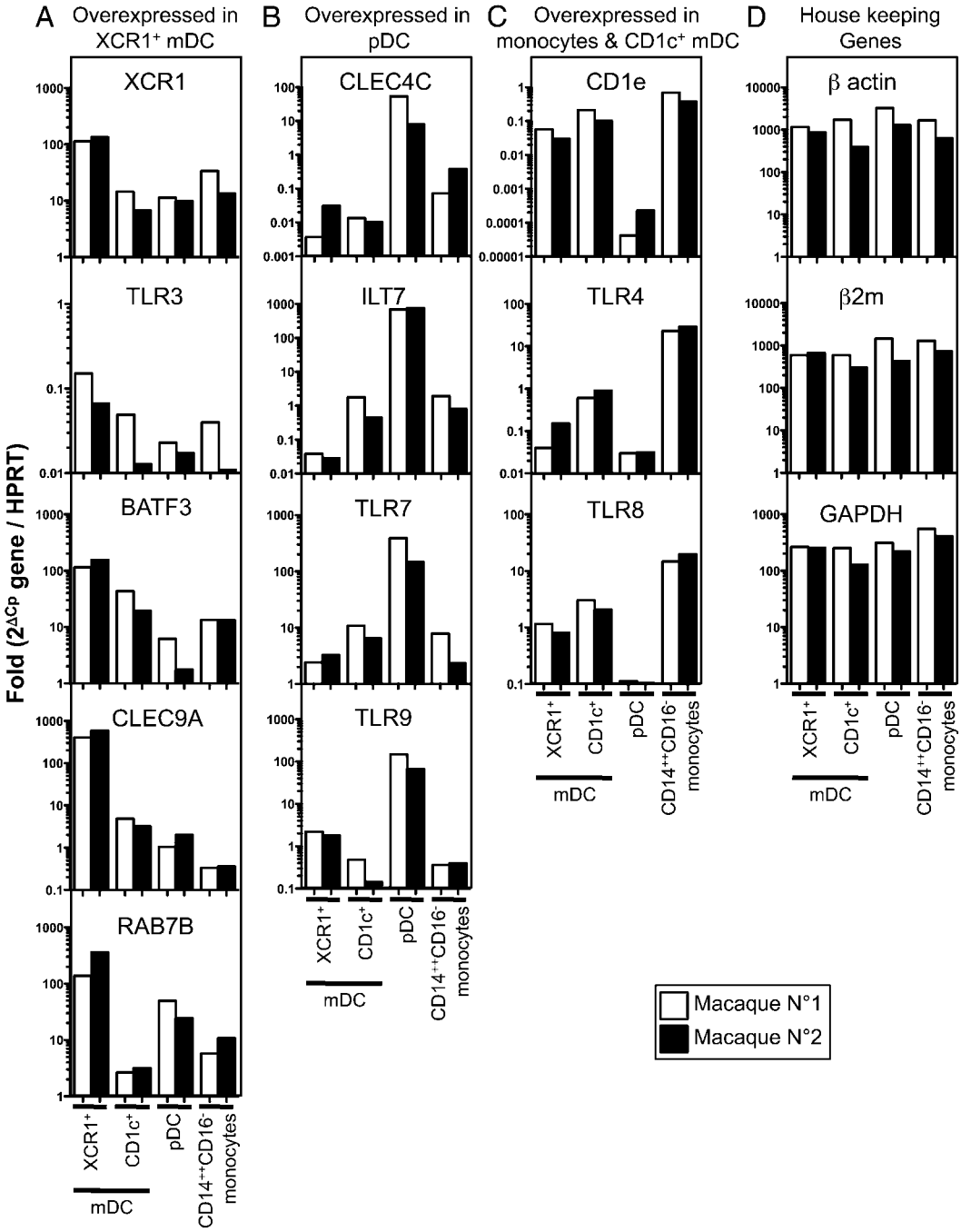

FIGURE 3. Quantification of mRNA from genes characteristic for human or murine XCR1$^+$ mDC, pDC, and monocytes in sorted rhesus macaque spleen cell populations. (**A**–**D**) Total cellular RNA from FACS-sorted lin$^-$MHC-II$^+$CADM1$^+$XCR1$^+$ mDC, lin$^-$MHC-II^{hi}CD1c$^+$ mDC, lin$^-$MHC-II^{lo}CD123$^+$ pDC, and CD14^{++}CD16$^-$ monocytes from two uninfected macaques were reverse transcribed and analyzed for expression by real-time PCR. Results are displayed for each gene as fold differences compared with the weakly expressed housekeeping gene *HPRT* using the 2eΔCp method. Results obtained for genes known to be differentially expressed by human and mouse XCR1$^+$ mDC (A), human and mouse pDC (B), human and mouse monocytes and conventional mDC (C), and for housekeeping genes (D) are displayed.

must ensure that like their human and murine counterparts, simian XCR1$^+$ mDC do perform cross presentation. This will require effector CD8$^+$ T cells specific for SIV epitopes, which can be obtained and characterized from infected or vaccinated macaques, and purified XCR1$^+$ cells to cross present the corresponding epitopes from an uninfected macaque expressing the same Mamu class I molecule restricting the response to these epitopes.

Most studies performed in macaques, in particular in the context of SIV infection, have defined mDC as being phenotypically similar to human mDC as lin(CD3/CD14/CD20)^{neg} MHC-II$^+$CD11c$^+$ cells, without excluding CD16$^+$ cells, because some macaque mDC express CD16 and low levels of CD11b (41, 45). Intriguingly, in these studies, and contrary to human and mouse mDC that express high levels of MHC-II molecules, in the blood and spleen, macaque mDC only expressed intermediate levels of MHC-II (tested with anti–HLA-DR Ab), whereas most CD11c^{neg} events among lin^{neg}CD123^{neg} cells had strong MHC-II expression levels but were not considered as mDC (41).

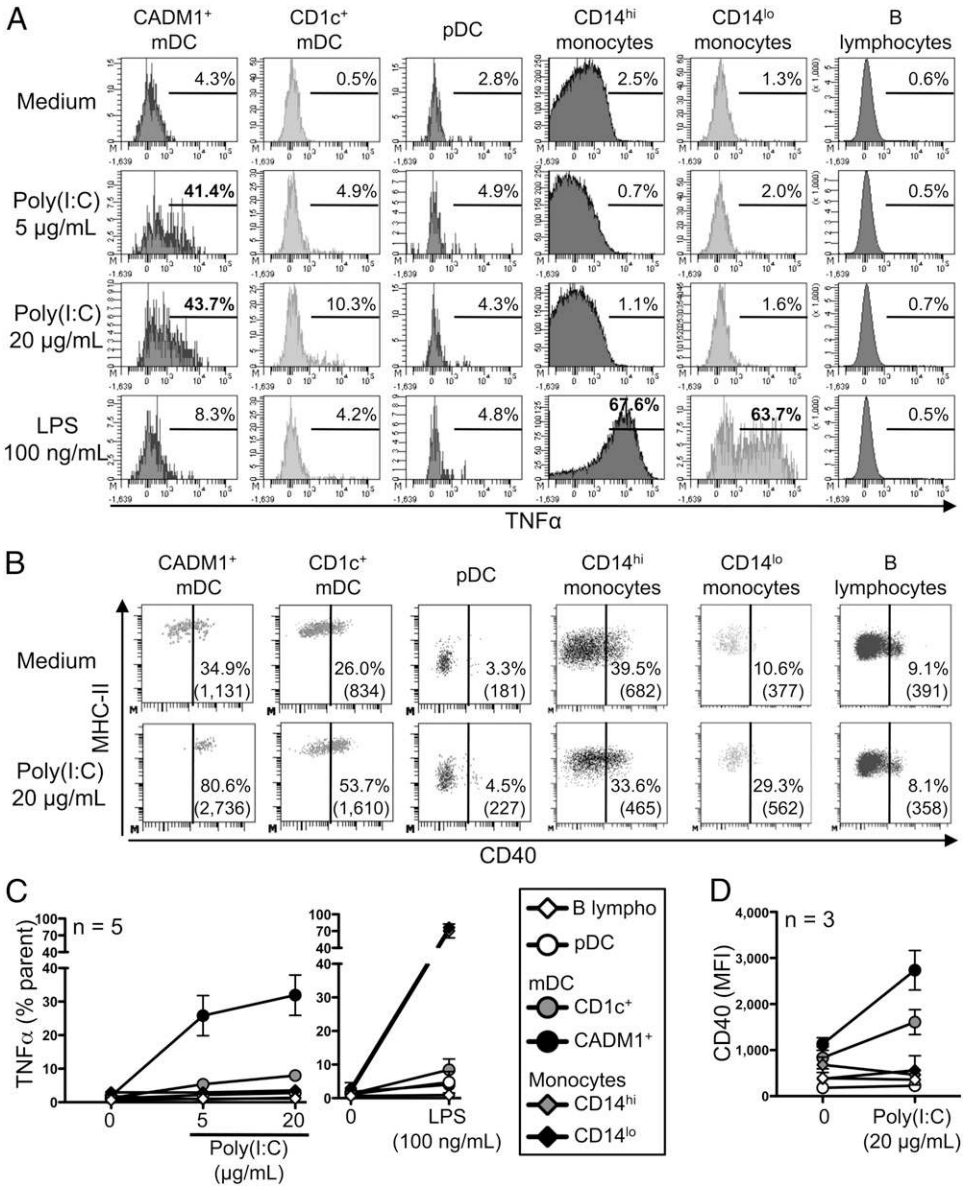

FIGURE 4. XCR1$^+$CADM1$^+$ mDC response to TLR3 triggering. (**A**) Histograms of the intracellular TNF-α FACS analysis from one healthy macaque showing TNF-α production in different DC and monocyte subsets after stimulation of PBMC with medium, poly(I:C), or LPS. The different cell subsets were defined as in Fig. 1A but without CD16 for monocyte subsets, the CD16 Ab being replaced by the anti–TNF-α Ab. Monocytes were therefore only defined as MHC-II$^+$, CD14^{hi}, and CD14^{lo} subsets. Percentages of TNF-α–positive cells among the parent population are indicated. (**B**) Flow cytometric dot plots showing MHC-II and CD40 expression by the different DC and monocyte subsets stimulated or not with poly(I:C). (**C**) Percentages of TNF-α–positive cells among the parent population in the different cell subsets stimulated or not with poly(I:C) or LPS. $n = 5$ healthy macaques. (**D**) CD40 labeling intensity in the different cell subsets stimulated or not with poly(I:C) (20 μg/ml). $n = 3$ healthy macaques. Bars indicate SEM.

We confirm in this study the previous observation that macaque CD1c$^+$ mDC express low levels of CD11c (59) and found that CD16$^+$ monocytes, and particularly the minor nonclassical CD14$^{+/-}$CD16^{++} subset, expressed the highest CD11c levels among PBMC and SMC. Therefore, previous studies analyzing lin^{neg}CD11c$^+$ mDC counts and proportions in the blood and spleen most probably included some CD16$^+$ monocytes, particularly nonclassical monocytes that weakly express CD14 and therefore fall into the lin^{neg} gate. It remains possible that macaque mDC might still express highly CD11c in other tissues. This precise delineation of monocyte and DC subsets will help settle down previous discrepancies about their variations during physiological or pathological conditions.

As an illustration, our cross-sectional analysis during acute infection, a stage that cannot be examined in humans, especially in lymphoid organs, shows a sharp increase of the absolute numbers of circulating XCR1$^+$ mDC during the first week of infection. The negative correlation of this increase with viral loads may indicate a specific susceptibility of CADM1$^+$ mDC to this viral infection and direct cytotoxicity, and not homing to lymphoid organs, because their proportions in the spleens also tended to correlate negatively with pVL. Alternatively, inflammation, in particular IL-12 (63) and/or IL-18, might promote the development of XCR1$^+$ DC, as recently reported in BATF3$^{-/-}$ mice, through the induction of other transcription factors with a partially redundant role for cell-type specification (64). Indeed, CD1c$^+$ mDC, pDC, and monocyte proportions also tended to be elevated in the blood during the first week of infection, as previously described (43, 45, 46, 48). Conversely, during chronic infection or AIDS, the proportions of XCR1$^+$ mDC were lower than in controls in blood and spleen, confirming our observations in viremic, chronically HIV-infected patients (35). A consequence of the CD1c$^+$ and XCR1$^+$ mDC number elevation during acute infection may be the induction of the CD8$^+$ T cell responses that are known to occur early; it may also be their destruction, and that of CD4$^+$ T cells, by these specific CD8$^+$ T cells as well as by other cell death effectors induced by HIV-1 infection (65). The consequence of the loss of CD1c$^+$ and XCR1$^+$ mDC from blood as well as from lymphoid organs during chronic infection may be that Ag presentation, and particularly cross-presentation, is compromised, unless pDC or inflammatory DC relay this function (66, 67).

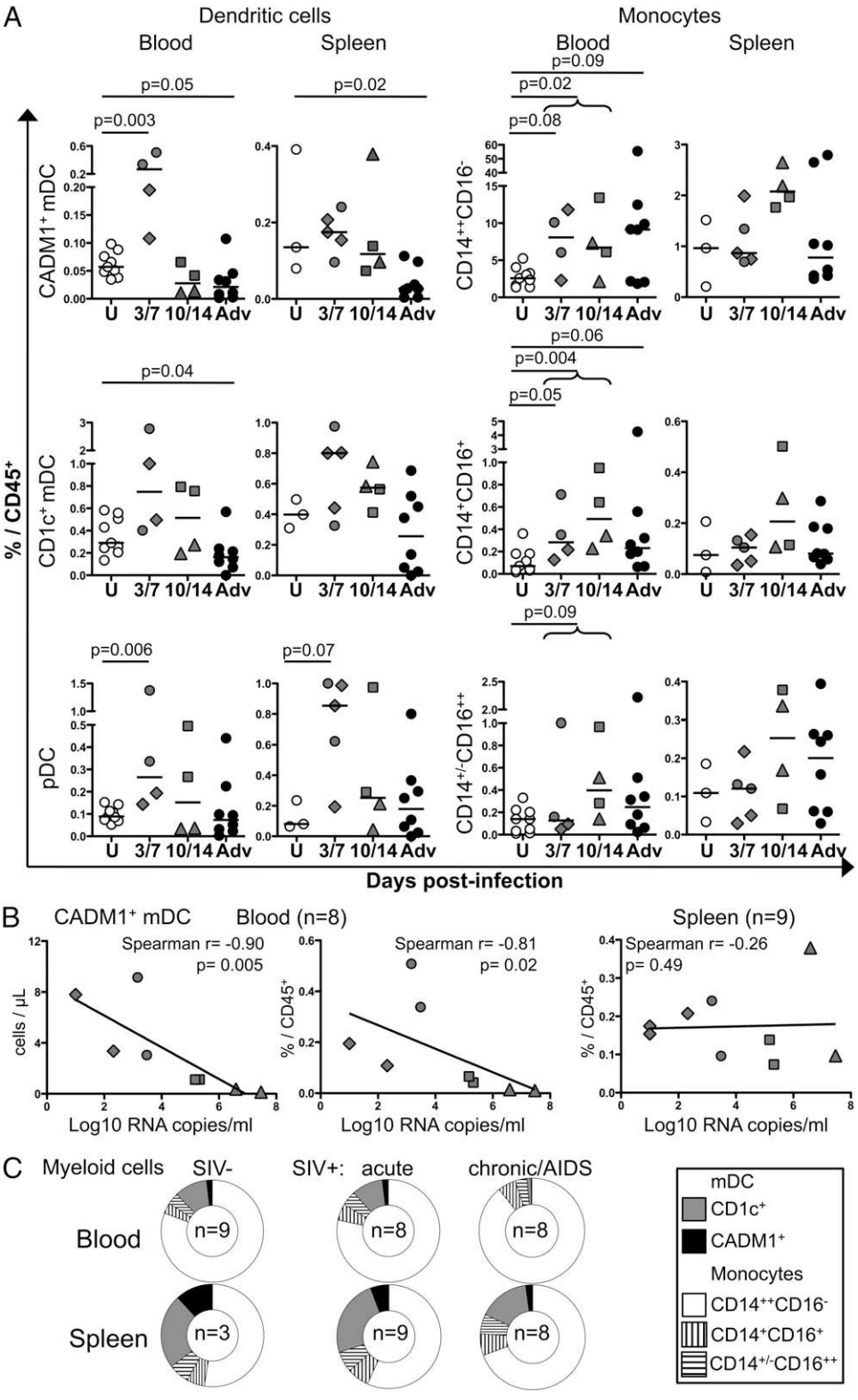

FIGURE 5. Monocyte and DC subset proportions during SIV infection. (**A**) Percentage among CD45$^+$ mononuclear cells of DC (*left panels*) and monocyte subsets (*right panels*) in the blood and spleen of uninfected macaques (U; open circles; $n = 9$) compared with macaques during SIV infection (gray and black symbols). Macaques analyzed at day 3 and day 7 (3/7; day 3, diamonds, blood: $n = 2$; spleen: $n = 3$; day 7, circles, $n = 2$) and day 10 and day 14 (10/14; day 10, squares, $n = 2$; day 14, triangles, $n = 2$) postinfection are displayed. Macaques with advanced infection (Adv; blood: $n = 8$; spleen: $n = 8$) are displayed as black circles. p values were calculated using the Mann–Whitney U test. (**B**) Correlation with viral loads of the absolute counts or percentage among CD45$^+$ mononuclear cells of CADM1$^+$ mDC in blood or spleen during acute infection [symbols used to defined different time postinfection are the same as in (A)]. Correlations were evaluated using the Spearman test. (**C**) Ring graphical representation of the mean proportion of mDC and monocyte subsets among total myeloid mononuclear cells in the blood and spleens from uninfected macaques that were sacrificed during acute or advanced infection.

Future studies will define XCR1$^+$ mDC in other organs such as gut-associated tissues and evaluate their functions in vivo in the context of SIV infection. Most importantly, identification of the equivalent of human XCR1$^+$CD141$^+$ and murine XCR1$^+$ CD8α^+ mDC will allow preclinical vaccinal studies targeting this population in a primate model close to humans, possibly in the bivalent vaccibody format (i.e., Ags linked to the chemokine ligand of XCR1, XCL1) (53, 54), and potential immunotherapies designed to compensate their loss during chronic HIV-1 infection.

Acknowledgments

We thank the other members of the Antigen Presentation by Dendritic Cell team and of the Agence Nationale de Recherches sur le Sida AC 31 for discussions. We also thank the Cochin Immunobiology Facility for maintaining the flow cytometers used for analyses and sorting.

Disclosures

E.F. and B.B. are inventors on a patent application for Xcl1-targeted vaccibodies. The other authors have no financial conflicts of interest.

References

1. Hildner, K., B. T. Edelson, W. E. Purtha, M. Diamond, H. Matsushita, M. Kohyama, B. Calderon, B. U. Schraml, E. R. Unanue, M. S. Diamond, et al. 2008. Batf3 deficiency reveals a critical role for CD8alpha+ dendritic cells in cytotoxic T cell immunity. *Science* 322: 1097–1100.
2. Kurts, C., B. W. Robinson, and P. A. Knolle. 2010. Cross-priming in health and disease. *Nat. Rev. Immunol.* 10: 403–414.
3. Lauterbach, H., B. Bathke, S. Gilles, C. Traidl-Hoffmann, C. A. Luber, G. Fejer, M. A. Freudenberg, G. M. Davey, D. Vremec, A. Kallies, et al. 2010. Mouse CD8alpha+ DCs and human BDCA3+ DCs are major producers of IFN-lambda in response to poly IC. *J. Exp. Med.* 207: 2703–2717.
4. Lahoud, M. H., F. Ahmet, J. G. Zhang, S. Meuter, A. N. Policheni, S. Kitsoulis, C. N. Lee, M. O'Keeffe, L. C. Sullivan, A. G. Brooks, et al. 2012. DEC-205 is a cell surface receptor for CpG oligonucleotides. *Proc. Natl. Acad. Sci. USA* 109: 16270–16275.
5. Zhang, J. G., P. E. Czabotar, A. N. Policheni, I. Caminschi, S. S. Wan, S. Kitsoulis, K. M. Tullett, A. Y. Robin, R. Brammananth, M. F. van Delft, et al. 2012. The dendritic cell receptor Clec9A binds damaged cells via exposed actin filaments. *Immunity* 36: 646–657.
6. Bachem, A., S. Güttler, E. Hartung, F. Ebstein, M. Schaefer, A. Tannert, A. Salama, K. Movassaghi, C. Opitz, H. W. Mages, et al. 2010. Superior antigen cross-presentation and XCR1 expression define human CD11c+CD141+ cells as homologues of mouse CD8+ dendritic cells. *J. Exp. Med.* 207: 1273–1281.
7. Crozat, K., R. Guiton, V. Contreras, V. Feuillet, C. A. Dutertre, E. Ventre, T. P. Vu Manh, T. Baranek, A. K. Storset, J. Marvel, et al. 2010. The XC chemokine receptor 1 is a conserved selective marker of mammalian cells homologous to mouse CD8alpha+ dendritic cells. *J. Exp. Med.* 207: 1283–1292.
8. Galibert, L., G. S. Diemer, Z. Liu, R. S. Johnson, J. L. Smith, T. Walzer, M. R. Comeau, C. T. Rauch, M. F. Wolfson, R. A. Sorensen, et al. 2005. Nectin-like protein 2 defines a subset of T-cell zone dendritic cells and is a ligand for class-I-restricted T-cell-associated molecule. *J. Biol. Chem.* 280: 21955–21964.
9. Sancho, D., O. P. Joffre, A. M. Keller, N. C. Rogers, D. Martínez, P. Hernanz-Falcón, I. Rosewell, and C. Reis e Sousa. 2009. Identification of a dendritic cell receptor that couples sensing of necrosis to immunity. *Nature* 458: 899–903.
10. MacDonald, K. P., D. J. Munster, G. J. Clark, A. Dzionek, J. Schmitz, and D. N. Hart. 2002. Characterization of human blood dendritic cell subsets. *Blood* 100: 4512–4520.
11. Poulin, L. F., M. Salio, E. Griessinger, F. Anjos-Afonso, L. Craciun, J. L. Chen, A. M. Keller, O. Joffre, S. Zelenay, E. Nye, et al. 2010. Characterization of human DNGR-1+ BDCA3+ leukocytes as putative equivalents of mouse CD8alpha+ dendritic cells. *J. Exp. Med.* 207: 1261–1271.
12. Jongbloed, S. L., A. J. Kassianos, K. J. McDonald, G. J. Clark, X. Ju, C. E. Angel, C. J. Chen, P. R. Dunbar, R. B. Wadley, V. Jeet, et al. 2010. Human CD141+ (BDCA-3)+ dendritic cells (DCs) represent a unique myeloid DC subset that cross-presents necrotic cell antigens. *J. Exp. Med.* 207: 1247–1260.
13. Robbins, S. H., T. Walzer, D. Dembélé, C. Thibault, A. Defays, G. Bessou, H. Xu, E. Vivier, M. Sellars, P. Pierre, et al. 2008. Novel insights into the relationships between dendritic cell subsets in human and mouse revealed by genome-wide expression profiling. *Genome Biol.* 9: R17.
14. Contreras, V., C. Urien, R. Guiton, Y. Alexandre, T. P. Vu Manh, T. Andrieu, K. Crozat, L. Jouneau, N. Bertho, M. Epardaud, et al. 2010. Existence of CD8α-like dendritic cells with a conserved functional specialization and a common molecular signature in distant mammalian species. *J. Immunol.* 185: 3313–3325.
15. Haniffa, M., A. Shin, V. Bigley, N. McGovern, P. Teo, P. See, P. S. Wasan, X. N. Wang, F. Malinarich, B. Malleret, et al. 2012. Human tissues contain CD141hi cross-presenting dendritic cells with functional homology to mouse CD103+ nonlymphoid dendritic cells. *Immunity* 37: 60–73.
16. Joffre, O. P., E. Segura, A. Savina, and S. Amigorena. 2012. Cross-presentation by dendritic cells. *Nat. Rev. Immunol.* 12: 557–569.
17. Mittag, D., A. I. Proietto, T. Loudovaris, S. I. Mannering, D. Vremec, K. Shortman, L. Wu, and L. C. Harrison. 2011. Human dendritic cell subsets from spleen and blood are similar in phenotype and function but modified by donor health status. *J. Immunol.* 186: 6207–6217.
18. Segura, E., M. Durand, and S. Amigorena. 2013. Similar antigen cross-presentation capacity and phagocytic functions in all freshly isolated human lymphoid organ-resident dendritic cells. *J. Exp. Med.* 210: 1035–1047.
19. Sancho, D., D. Mourão-Sá, O. P. Joffre, O. Schulz, N. C. Rogers, D. J. Pennington, J. R. Carlyle, and C. Reis e Sousa. 2008. Tumor therapy in mice via antigen targeting to a novel, DC-restricted C-type lectin. *J. Clin. Invest.* 118: 2098–2110.
20. Bonifaz, L. C., D. P. Bonnyay, A. Charalambous, D. I. Darguste, S. Fujii, H. Soares, M. K. Brimnes, B. Moltedo, T. M. Moran, and R. M. Steinman. 2004. In vivo targeting of antigens to maturing dendritic cells via the DEC-205 receptor improves T cell vaccination. *J. Exp. Med.* 199: 815–824.
21. Meixlsperger, S., C. S. Leung, P. C. Rämer, M. Pack, L. D. Vanoaica, G. Breton, S. Pascolo, A. M. Salazar, A. Dzionek, J. Schmitz, et al. 2013. CD141+ dendritic cells produce prominent amounts of IFN-α after dsRNA recognition and can be targeted via DEC-205 in humanized mice. *Blood* 121: 5034–5044.
22. Flynn, B. J., K. Kastenmüller, U. Wille-Reece, G. D. Tomaras, M. Alam, R. W. Lindsay, A. M. Salazar, B. Perdiguero, C. E. Gomez, R. Wagner, et al. 2011. Immunization with HIV Gag targeted to dendritic cells followed by recombinant New York vaccinia virus induces robust T-cell immunity in nonhuman primates. *Proc. Natl. Acad. Sci. USA* 108: 7131–7136.
23. Kato, M., K. J. McDonald, S. Khan, I. L. Ross, S. Vuckovic, K. Chen, D. Munster, K. P. MacDonald, and D. N. Hart. 2006. Expression of human DEC-205 (CD205) multilectin receptor on leukocytes. *Int. Immunol.* 18: 857–869.
24. Ruprecht, R. M. 1999. Live attenuated AIDS viruses as vaccines: promise or peril? *Immunol. Rev.* 170: 135–149.
25. Chehimi, J., D. E. Campbell, L. Azzoni, D. Bacheller, E. Papasavvas, G. Jerandi, K. Mounzer, J. Kostman, G. Trinchieri, and L. J. Montaner. 2002. Persistent decreases in blood plasmacytoid dendritic cell number and function despite effective highly active antiretroviral therapy and increased blood myeloid dendritic cells in HIV-infected individuals. *J. Immunol.* 168: 4796–4801.
26. Dillon, S. M., L. J. Friedlander, L. M. Rogers, A. L. Meditz, J. M. Folkvord, E. Connick, M. D. McCarter, and C. C. Wilson. 2011. Blood myeloid dendritic cells from HIV-1-infected individuals display a proapoptotic profile characterized by decreased Bcl-2 levels and by caspase-3+ frequencies that are associated with levels of plasma viremia and T cell activation in an exploratory study. *J. Virol.* 85: 397–409.
27. Grassi, F., A. Hosmalin, D. McIlroy, V. Calvez, P. Debré, and B. Autran. 1999. Depletion in blood CD11c-positive dendritic cells from HIV-infected patients. *AIDS* 13: 759–766.
28. Pacanowski, J., S. Kahi, M. Baillet, P. Lebon, C. Deveau, C. Goujard, L. Meyer, E. Oksenhendler, M. Sinet, and A. Hosmalin. 2001. Reduced blood CD123+ (lymphoid) and CD11c+ (myeloid) dendritic cell numbers in primary HIV-1 infection. *Blood* 98: 3016–3021.
29. Sabado, R. L., M. O'Brien, A. Subedi, L. Qin, N. Hu, E. Taylor, O. Dibben, A. Stacey, J. Fellay, K. V. Shianna, et al. 2010. Evidence of dysregulation of dendritic cells in primary HIV infection. *Blood* 116: 3839–3852.
30. Smed-Sörensen, A., and K. Loré. 2011. Dendritic cells at the interface of innate and adaptive immunity to HIV-1. *Curr. Opin. HIV AIDS* 6: 405–410.
31. Chen, J., A. Benlahrech, P. Kelleher, and S. Patterson. 2013. Increased Activity of Extrinsic and Intrinsic Apoptosis Pathways in Different Mononuclear Cell Types in HIV Type 1-Infected Patients Regardless of Whether They Are Depleted in Disease. *AIDS Res. Hum. Retroviruses* 29: 709–717.
32. Donaghy, H., A. Pozniak, B. Gazzard, N. Qazi, J. Gilmour, F. Gotch, and S. Patterson. 2001. Loss of blood CD11c(+) myeloid and CD11c(-) plasmacytoid dendritic cells in patients with HIV-1 infection correlates with HIV-1 RNA virus load. *Blood* 98: 2574–2576.
33. Servet, C., L. Zitvogel, and A. Hosmalin. 2002. Dendritic cells in innate immune responses against HIV. *Curr. Mol. Med.* 2: 739–756.
34. Soumelis, V., I. Scott, F. Gheyas, D. Bouhour, G. Cozon, L. Cotte, L. Huang, J. A. Levy, and Y. J. Liu. 2001. Depletion of circulating natural type 1 interferon-producing cells in HIV-infected AIDS patients. *Blood* 98: 906–912.
35. Dutertre, C. A., S. Amraoui, A. DeRosa, J. P. Jourdain, L. Vimeux, M. Goguet, S. Degrelle, V. Feuillet, A. S. Liovat, M. Müller-Trutwin, et al. 2012. Pivotal role of M-DC8^{+} monocytes from viremic HIV-infected patients in TNFα overproduction in response to microbial products. *Blood* 120: 2259–2268.
36. Cros, J., N. Cagnard, K. Woollard, N. Patey, S. Y. Zhang, B. Senechal, A. Puel, S. K. Biswas, D. Moshous, C. Picard, et al. 2010. Human CD14dim monocytes patrol and sense nucleic acids and viruses via TLR7 and TLR8 receptors. *Immunity* 33: 375–386.
37. Ziegler-Heitbrock, L., P. Ancuta, S. Crowe, M. Dalod, V. Grau, D. N. Hart, P. J. Leenen, Y. J. Liu, G. MacPherson, G. J. Randolph, et al. 2010. Nomenclature of monocytes and dendritic cells in blood. *Blood* 116: e74–e80.
38. Thieblemont, N., L. Weiss, H. M. Sadeghi, C. Estcourt, and N. Haeffner-Cavaillon. 1995. CD14lowCD16high: a cytokine-producing monocyte subset which expands during human immunodeficiency virus infection. *Eur. J. Immunol.* 25: 3418–3424.
39. Ancuta, P., A. Kamat, K. J. Kunstman, E. Y. Kim, P. Autissier, A. Wurcel, T. Zaman, D. Stone, M. Mefford, S. Morgello, et al. 2008. Microbial translocation is associated with increased monocyte activation and dementia in AIDS patients. *PLoS ONE* 3: e2516.
40. Hearps, A. C., A. Maisa, W. J. Cheng, T. A. Angelovich, G. F. Lichtfuss, C. S. Palmer, A. L. Landay, A. Jaworowski, and S. M. Crowe. 2012. HIV infection induces age-related changes to monocytes and innate immune activation in young men that persist despite combination antiretroviral therapy. *AIDS* 26: 843–853.
41. Brown, K. N., A. Trichel, and S. M. Barratt-Boyes. 2007. Parallel loss of myeloid and plasmacytoid dendritic cells from blood and lymphoid tissue in simian AIDS. *J. Immunol.* 178: 6958–6967.
42. Brown, K. N., V. Wijewardana, X. Liu, and S. M. Barratt-Boyes. 2009. Rapid influx and death of plasmacytoid dendritic cells in lymph nodes mediate depletion in acute simian immunodeficiency virus infection. *PLoS Pathog.* 5: e1000413.
43. Malleret, B., B. Manéglier, I. Karlsson, P. Lebon, M. Nascimbeni, L. Perié, P. Brochard, B. Delache, J. Calvo, T. Andrieu, et al. 2008. Primary infection with simian immunodeficiency virus: plasmacytoid dendritic cell homing to lymph nodes, type I interferon, and immune suppression. *Blood* 112: 4598–4608.
44. Malleret, B., I. Karlsson, B. Manéglier, P. Brochard, B. Delache, T. Andrieu, M. Muller-Trutwin, T. Beaumont, J. M. McCune, J. Banchereau, et al. 2008. Effect of SIVmac infection on plasmacytoid and CD1c+ myeloid dendritic cells in cynomolgus macaques. *Immunology* 124: 223–233.
45. Wijewardana, V., A. C. Soloff, X. Liu, K. N. Brown, and S. M. Barratt-Boyes. 2010. Early myeloid dendritic cell dysregulation is predictive of disease progression in simian immunodeficiency virus infection. *PLoS Pathog.* 6: e1001235.
46. Otani, I., H. Akari, K. H. Nam, K. Mori, E. Suzuki, H. Shibata, K. Doi, K. Terao, and Y. Yosikawa. 1998. Phenotypic changes in peripheral blood monocytes of cynomolgus monkeys acutely infected with simian immunodeficiency virus. *AIDS Res. Hum. Retroviruses* 14: 1181–1186.

47. Kim, W. K., Y. Sun, H. Do, P. Autissier, E. F. Halpern, M. Piatak, Jr., J. D. Lifson, T. H. Burdo, M. S. McGrath, and K. Williams. 2010. Monocyte heterogeneity underlying phenotypic changes in monocytes according to SIV disease stage. *J. Leukoc. Biol.* 87: 557–567.
48. Burdo, T. H., C. Soulas, K. Orzechowski, J. Button, A. Krishnan, C. Sugimoto, X. Alvarez, M. J. Kuroda, and K. C. Williams. 2010. Increased monocyte turnover from bone marrow correlates with severity of SIV encephalitis and CD163 levels in plasma. *PLoS Pathog.* 6: e1000842.
49. Gama, L., E. N. Shirk, J. N. Russell, K. I. Carvalho, M. Li, S. E. Queen, J. Kalil, M. C. Zink, J. E. Clements, and E. G. Kallas. 2012. Expansion of a subset of CD14highCD16negCCR2low/neg monocytes functionally similar to myeloid-derived suppressor cells during SIV and HIV infection. *J. Leukoc. Biol.* 91: 803–816.
50. Wonderlich, E. R., V. Wijewardana, X. Liu, and S. M. Barratt-Boyes. 2013. Virus-encoded TLR ligands reveal divergent functional responses of mononuclear phagocytes in pathogenic simian immunodeficiency virus infection. *J. Immunol.* 190: 2188–2198.
51. Parker, R., J. Dutrieux, S. Beq, B. Lemercier, S. Rozlan, V. Fabre-Mersseman, M. Rancez, C. Gommet, B. Assouline, I. Rancé, et al. 2010. Interleukin-7 treatment counteracts IFN-α therapy-induced lymphopenia and stimulates SIV-specific cytotoxic T lymphocyte responses in SIV-infected rhesus macaques. *Blood* 116: 5589–5599.
52. Crozat, K., S. Tamoutounour, T. P. Vu Manh, E. Fossum, H. Luche, L. Ardouin, M. Guilliams, H. Azukizawa, B. Bogen, B. Malissen, et al. 2011. Cutting edge: expression of XCR1 defines mouse lymphoid-tissue resident and migratory dendritic cells of the CD8α+ type. *J. Immunol.* 187: 4411–4415.
53. Fredriksen, A. B., I. Sandlie, and B. Bogen. 2006. DNA vaccines increase immunogenicity of idiotypic tumor antigen by targeting novel fusion proteins to antigen-presenting cells. *Mol. Ther.* 13: 776–785.
54. Fredriksen, A. B., and B. Bogen. 2007. Chemokine-idiotype fusion DNA vaccines are potentiated by bivalency and xenogeneic sequences. *Blood* 110: 1797–1805.
55. Øynebråten, I., T. O. Løvås, K. Thompson, and B. Bogen. 2012. Generation of antibody-producing hybridomas following one single immunization with a targeted DNA vaccine. *Scand. J. Immunol.* 75: 379–388.
56. Dion, M. L., J. F. Poulin, R. Bordi, M. Sylvestre, R. Corsini, N. Kettaf, A. Dalloul, M. R. Boulassel, P. Debré, J. P. Routy, et al. 2004. HIV infection rapidly induces and maintains a substantial suppression of thymocyte proliferation. *Immunity* 21: 757–768.
57. Dion, M. L., R. P. Sékaly, and R. Cheynier. 2007. Estimating thymic function through quantification of T-cell receptor excision circles. *Methods Mol. Biol.* 380: 197–213.
58. Huysamen, C., J. A. Willment, K. M. Dennehy, and G. D. Brown. 2008. CLEC9A is a novel activation C-type lectin-like receptor expressed on BDCA3+ dendritic cells and a subset of monocytes. *J. Biol. Chem.* 283: 16693–16701.
59. Autissier, P., C. Soulas, T. H. Burdo, and K. C. Williams. 2010. Immunophenotyping of lymphocyte, monocyte and dendritic cell subsets in normal rhesus macaques by 12-color flow cytometry: clarification on DC heterogeneity. *J. Immunol. Methods* 360: 119–128.
60. Crozat, K., E. Vivier, and M. Dalod. 2009. Crosstalk between components of the innate immune system: promoting anti-microbial defenses and avoiding immunopathologies. *Immunol. Rev.* 227: 129–149.
61. Zelenay, S., A. M. Keller, P. G. Whitney, B. U. Schraml, S. Deddouche, N. C. Rogers, O. Schulz, D. Sancho, and C. Reis e Sousa. 2012. The dendritic cell receptor DNGR-1 controls endocytic handling of necrotic cell antigens to favor cross-priming of CTLs in virus-infected mice. *J. Clin. Invest.* 122: 1615–1627.
62. Poulin, L. F., Y. Reyal, H. Uronen-Hansson, B. U. Schraml, D. Sancho, K. M. Murphy, U. K. Håkansson, L. F. Moita, W. W. Agace, D. Bonnet, and C. Reis e Sousa. 2012. DNGR-1 is a specific and universal marker of mouse and human Batf3-dependent dendritic cells in lymphoid and nonlymphoid tissues. *Blood* 119: 6052–6062.
63. Louis, S., C. A. Dutertre, L. Vimeux, L. Fery, L. Henno, S. Diocou, S. Kahi, C. Deveau, L. Meyer, C. Goujard, and A. Hosmalin. 2010. IL-23 and IL-12p70 production by monocytes and dendritic cells in primary HIV-1 infection. *J. Leukoc. Biol.* 87: 645–653.
64. Tussiwand, R., W. L. Lee, T. L. Murphy, M. Mashayekhi, K. C. Wumesh, J. C. Albring, A. T. Satpathy, J. A. Rotondo, B. T. Edelson, N. M. Kretzer, et al. 2012. Compensatory dendritic cell development mediated by BATF-IRF interactions. *Nature* 490: 502–507.
65. Lichtner, M., C. Marañón, P. O. Vidalain, O. Azocar, D. Hanau, P. Lebon, M. Burgard, C. Rouzioux, V. Vullo, H. Yagita, et al. 2004. HIV type 1-infected dendritic cells induce apoptotic death in infected and uninfected primary CD4 T lymphocytes. *AIDS Res. Hum. Retroviruses* 20: 175–182.
66. Hoeffel, G., A. C. Ripoche, D. Matheoud, M. Nascimbeni, N. Escriou, P. Lebon, F. Heshmati, J. G. Guillet, M. Gannagé, S. Caillat-Zucman, et al. 2007. Antigen crosspresentation by human plasmacytoid dendritic cells. *Immunity* 27: 481–492.
67. Segura, E., M. Touzot, A. Bohineust, A. Cappuccio, G. Chiocchia, A. Hosmalin, M. Dalod, V. Soumelis, and S. Amigorena. 2013. Human inflammatory dendritic cells induce Th17 cell differentiation. *Immunity* 38: 336–348.